

MULTI-FIDELITY ROBUST DESIGN OPTIMIZATION OF AN ORC TURBINE FOR HIGH TEMPERATURE WASTE-HEAT RECOVERY

Aldo Serafino^{1*}, Benoît Obert¹, Paola Cinnela²

¹Enertime, 1 rue du Moulin des Bruyères, 92400 Courbevoie, France

²Institute Jean le Rond d'Alembert, Sorbonne Université, 4 place de Jussieu, 75005 Paris, France

*Corresponding Author: aldo.serafino@enertime.com

ABSTRACT

The ORC technology is subject to manifold sources of uncertainty that can have a severe impact on the thermodynamic and economic efficiency of plant components, particularly when the system is operated at off-design conditions. In this contribution we focus on the development of ORC turbines with stable performance under uncertainty: a novel multi-fidelity robust design optimization (RDO) strategy is used to design the first nozzle of an ORC turbine for high temperature waste-heat recovery. For this kind of application, the turbine inlet and outlet conditions may vary randomly over a large range. The RDO strategy combines parsimonious uncertainty quantification techniques with a multi-objective genetic algorithm optimizer based on surrogate models. The multi-fidelity approach allows to estimate with high accuracy and with a low computational cost the statistical moments of the probability distribution function of the quantity of interest, which here is the entropy generation within the cascade. To improve the accuracy of the surrogate model coupled with the optimizer, the multi-objective expected improvement criterion is adopted. The optimization converges to an efficient optimum solution, ensuring improved and stable performance over the whole considered range of uncertain operating conditions and with a computational cost that is significantly lower than other RDO approaches proposed in literature.

1 INTRODUCTION

According to the estimation provided by the International Energy Agency, within the next 20 years we are likely to register a further increase in the world's population of 1.7 billion people, most of which is expected to be concentrated in urban areas of developing countries (IEA, 2018), leading to a dramatic rise in the demand for energy, goods, and services.

Such a forecast is confirmed by the study of trends over the past two decades, indicating that during this time range the demand for industrial products has increased significantly worldwide. This growth is mainly due to the rise of production in energy-intensive industrial sectors like iron and steel, cement, chemicals, glass, aluminum and paper and it indicates that global industry could become more energy intensive in the next years (Levi *et al.*, 2020).

Immediate measures are therefore necessary to curb the surge in energy consumption and to reduce carbon footprint; since energy efficiency plays a key role in accelerating the transition to sustainable energy (IEA, 2020), industrial waste heat recovery (WHR) should be considered as a key strategy to be exploited. Indeed, one has to consider that just in Europe an estimated potential of about 300 TWh/year is available for heat recovery from industrial processes (Papapetrou *et al.*, 2018, Bianchi *et al.*, 2019).

ORCs are a mature and effective technology for this purpose. However, despite many energy-intensive industries could benefit from the integration of an ORC, the employment of this technology continues to be limited. In fact, without the aim of providing an exhaustive list of ORCs for WHR, as of April 2021 Turboden declares about 86 MW of installed capacity (Turboden, 2021), Exergy about 31 MW (Exergy, 2021), Ormat 134 MW from gas compressor stations and only 15 MW from industrial applications (Ormat, 2021) and Enertime 11 MW.

One of the main reasons behind this reticence stems from the lack of confidence of potential investors, who still consider that the potential energy savings offered by a WHR application do not offset the risk

connected to the project (Mahmoudi *et al.*, 2018). Such a belief is nowadays unjustified and is rooted in a context that is no longer current, considering the measures lawmakers are taking worldwide (see for instance EU Parliament, 2018 or US Congress, 2021 or Liu, 2018).

Nevertheless, an industrial WHR project can be affected by several sources of uncertainty. Among them, the variability of the thermal input to be recovered is likely to be the most crucial one; in fact, despite the belief that thermal process in cement, glass and iron and steel industry is constant, some fluctuations in the mass flow rate and in the temperature of the exhaust gas usually occur with hourly, daily, monthly and yearly timescale as a consequence of:

- the variation of the production of the factory during the year (typically, seasonal production),
- the adaptation of the factory's production to the demand over the entire period of the WHR project,
- periodic burners reversal cycles in the factory's furnace (as in regenerative furnaces),
- eventual discontinuities in the factory's productive process.

This variability in the input power has a major impact over the ORC system used for the heat recovery and all its components. In particular, the turbine is the most critical equipment in this sense, since when it is operated in off-design condition far from the nominal point, it may drop in efficiency with a significant impact on the performance of the overall system and, consequently, the profitability of the whole WHR project.

To account for this uncertainty, some safety margins are typically used in the design of the ORC and its components. Still, this approach presents the risk of not being efficient from an energy and economic viewpoint. Hence, in such a context robust design optimization (RDO) should be considered as a promising alternative strategy to standard design methods, allowing to ensure more stable performance over a range of randomly varying operating conditions.

The present work presents the main results of the application of a novel multi-fidelity RDO methodology for the efficient 2D design of the first nozzle of an ORC turbine for high temperature WHR. In the following, Section 2 provides a description of the model of the turbine blade employed for the optimization, while Section 3 explains the adopted RDO strategy and section 4 shows the main results. Finally, conclusions and some perspectives are given in Section 5.

2 MODEL DESCRIPTION

The objective of the RDO here carried out is the shape optimization of the blade profile for the first nozzle of an ORC turbine for high temperature WHR applications. The working fluid is cyclopentane and the cascade is supposed to work under uncertain operating conditions, since the inlet total pressure $P_{T,in}$, the inlet total temperature $T_{T,in}$ and the outlet static pressure P_{out} are submitted to aleatory fluctuations. For the present test case, such sources of uncertainty are modelled by means of the Gaussian probability distribution functions (PDF) defined in Table 1, which reports the mean value of these three PDFs and their coefficient of variation, defined as the ratio between the mean value and the standard deviation. However, the adopted RDO strategy is general and can be straightforwardly applied even in case of different modelling of the uncertainty. The ranges of variation of the inlet/outlet conditions are represented in the h-s chart reported in Figure 1.

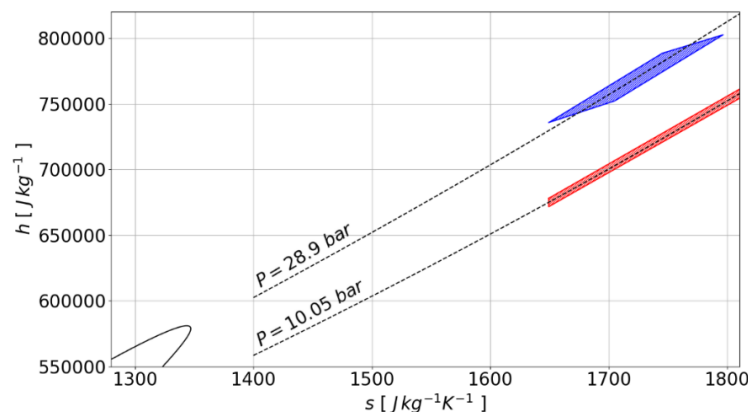


Figure 1: h-s chart with uncertainty at the inlet and at the outlet of the cascade

Table 1: Uncertain operating conditions

| Variable | PDF type | PDF mean value | Coefficient of variation |
|------------|----------|----------------|--------------------------|
| $P_{T,in}$ | Gaussian | 28.9 bar | 4.5% |
| $T_{T,in}$ | Gaussian | 277.3 degC | 0.6% |
| P_{out} | Gaussian | 10.05 bar | 2.0% |

The randomness of $P_{T,in}$ and $T_{T,in}$ determines an uncertainty at the inlet of the cascade that is identified with the blue hatched area, while P_{out} spans the red hatched area. The saturation curve on the lower left margin indicates that the working fluid is highly superheated.

For the design of the turbine blade, a family of candidate geometries is generated with the free-form deformation method (Sederberg, and Parry, 1986): a lattice of control points is used to deform the geometry of a baseline blade, by means of a bivariate tensor product of Bernstein polynomials.

As presented in Figure 2, for the present work, the lattice is made by 12 control points, named with letters A to L. To enforce the axial chord length and to avoid uncontrollable deformations of the trailing edge, the four corners (points A, F, G and L, colored in black) are constrained and only vertical displacements of the other 8 control points (colored in red) are allowed.

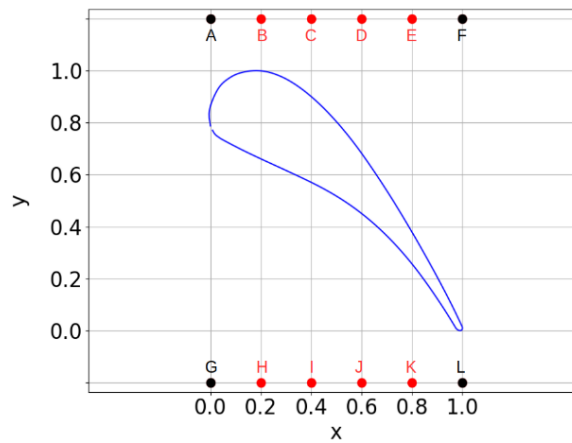


Figure 2: Blade profile parametrization with the FFD technique

Hence, this parametrization introduces eight design parameters, which are the vertical displacements δ of the eight free-form deformation control points: they can move, deforming the baseline profile to generate an optimal blade with improved performance. To avoid an excessive deformation of the profile during the RDO, the variation interval of the 8 design parameters has been bounded with the values δ_{MAX} and δ_{MIN} reported in Table 2.

To study the system, the open-source code GMSH (Geuzaine and Remacle, 2009) has been used to generate the computational grid, adopting the meshing strategy depicted in Figure 3: the domain presents an inlet surface (identified as A) an outlet surface (indicated as B) and two periodic surfaces (called C and D); the blade surface is noted as E. This strategy is employed to build three unstructured meshes with a different refinement: the coarse grid has 4772 elements, the medium has 16453 while the fine has 56885. To resolve viscous layers close to the blade walls, a boundary layer infill has been adopted, so that the maximum Y^+ value along the wall is always lower than 1.2. Moreover, since the trailing edge effects are important in the account of total losses, this region has been particularly refined. To reduce the RDO computational burden, the medium mesh will be used for all CFD simulations solved during the optimization. The independence of the solution from the computational grid will be then verified ex-post.

Table 2: Upper and lower boundary of the variation interval for the 8 design parameters

| Variable | B | C | D | E | H | I | J | K |
|----------------|-------|-----|-----|------|------|------|------|------|
| δ_{MIN} | -2.5% | -5% | -5% | -10% | -10% | -15% | -10% | -10% |
| δ_{MAX} | 2.5% | 5% | 5% | 10% | 10% | 15% | 10% | 10% |

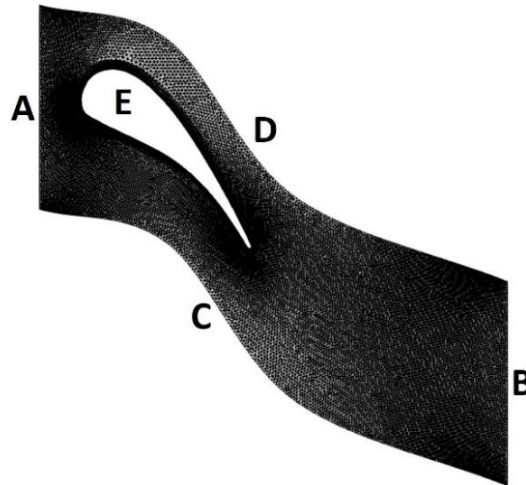


Figure 3: Mesh strategy used for the CFD simulation of the blade during the RDO (fine grid)

The flow is governed by the compressible Navier-Stokes equations, solved in a 2D Cartesian coordinate frame with the SU2 code (Economon *et al.*, 2016). The Jameson-Schmidt-Turkel central scheme (Jameson, 2017) has been used for the discretization of convective inviscid fluxes, while an Euler implicit method has been employed for time discretization and turbulent stresses are modelled with the SST k-omega RANS model (Menter, 1994). The linearized equations have been solved by means of the FGMRES method and an incomplete lower upper factorization with connectivity-based sparse pattern has been adopted as a linear pre-conditioner. Fluid properties are estimated with Peng-Robinson (Peng and Robinson, 1976) equation of state, while constant values are assumed for transport properties. As a convergence criterion, the order of magnitude of the RMS residuals for the mass, momentum (in both X and Y directions), and energy are set at 10^{-6} .

3 ROBUST DESIGN OPTIMIZATION STRATEGY

The adopted RDO methodology is represented in Figure 4: given the information about the PDF of the three uncertain variables, namely $P_{T,in}$, $T_{T,in}$ and P_{out} , and defined the eight design parameters, an uncertainty quantification (UQ) model can be exploited to estimate the PDF of the quantity of interest (QoI) J; more specifically, since Taguchi’s RDO criterion (Taguchi, 1987) is employed here, the aim of the optimization is to identify the best values of the 8 design parameters minimizing the expectancy and the standard deviation of the PDF of the QoI J, respectively called $E[J]$ and $STD[J]$.

In the present work, the average entropy difference between the outlet and the inlet of the domain is considered as the QoI J, since it is a convenient measure of internal flow losses affecting the adiabatic turbine expansion.

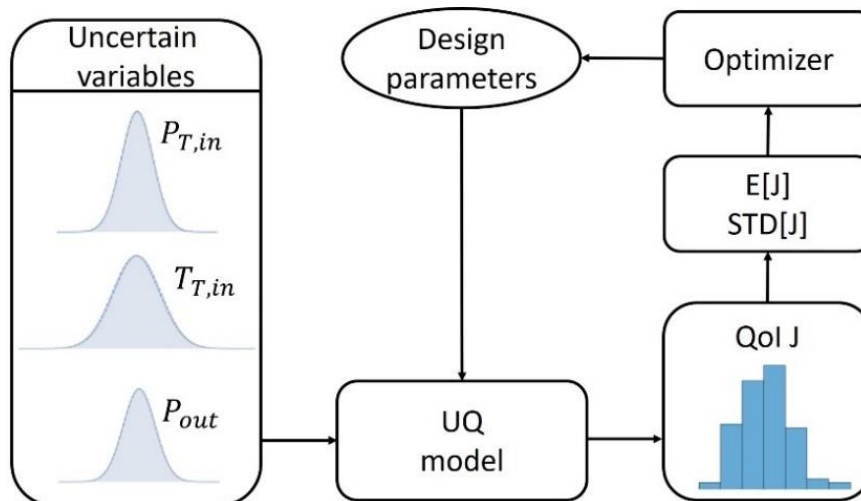


Figure 4: Workflow of the robust design optimization methodology

To lower the computational cost of the RDO, a multi-objective genetic algorithm optimizer (Deb, 2002) is coupled with the response surface of a surrogate model that is built by means of a multi-fidelity strategy. Such a response surface provides an estimation of $E[J]$ and $STD[J]$ and it is constructed leveraging the evaluations of the low-fidelity UQ model, which is cheap but inaccurate, with only few runs of the high-fidelity UQ model, that is more accurate but extremely expensive: this multi-fidelity approach allows to perform UQ estimations accurate as the high-fidelity model at the cost of the low-fidelity one. A detailed description of the present RDO strategy can be found in Serafino *et al.* (2020a). Specifically, here the first order method of moments (Hazelton, 2011) is used as low-fidelity UQ model and the Bayesian Kriging (Wikle and Berliner, 2007) as the high-fidelity one.

The first order method of moments uses the first order derivative of the QoI J with respect to the uncertain variables $P_{T,in}$, $T_{T,in}$ and P_{out} to provide an estimation of $E[J]$ and $STD[J]$; since in the present work a second-order central finite differences scheme has been used to estimate such a derivative, one UQ calculation with the low-fidelity method costs 7 CFD simulations.

For the high-fidelity UQ model, a small set of CFD calculations are required to construct the Bayesian Kriging response surface approximating the PDF of the QoI J in the space of the uncertain variables; then, this is used to estimate $E[J]$ and $STD[J]$. After some numerical experiments, it has come out that for this study 32 CFD calculations represent a good trade-off between accuracy and computational cost. 80 samples are considered for the construction of the low-fidelity design of experiments, while the high-fidelity one contains only 20 samples. Hence, the complete calculation of both designs of experiments requires respectively 560 and 640 CFD simulations. Once both datasets are constructed, the multi-fidelity approach is adopted to build the response surface to be coupled with the optimizer: on this surrogate, the multi-objective genetic algorithm initializes randomly a first population composed by 40 individuals in the design space which is let to evolve over 20 generations. To improve the accuracy of the surrogate, an adaptive infill is calculated every 5 generations with the multi-objective expected improvement criterion (Keane, 2006). The overall design process requires 1271 CFD simulations, which represents a considerable improvement compared to other RDO approaches proposed in literature (see Bufi and Cinnella, 2016, Serafino *et al.* 2020b or Razaaly *et al.*, 2020).

4 RESULTS

All solutions calculated during the optimization on the response surface of the surrogate coupled with the optimizer are plotted on the objective space $E[J]$ vs. $STD[J]$ depicted in Figure 5. From the analysis of the Pareto front, depicted as a black dashed line, it is possible to appreciate that solutions minimizing $E[J]$ maximize $STD[J]$. Therefore, a unique optimum solution does not exist, since it is not possible to minimize simultaneously both $E[J]$ and $STD[J]$. Among the optimal solutions lying on the Pareto front, the one offering the best compromise has been selected. This point, represented as a red symbol in Figure 5, is slightly shifted from the Pareto front, because after the optimization it has been re-evaluated with the high-fidelity model; as shown in Figure 5, the error of the surrogate coupled with the optimizer is lower than 2%.

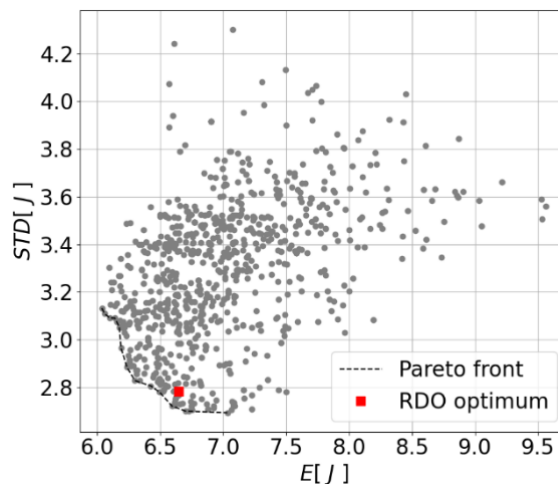


Figure 5: Objective space $E[J]$ – $STD[J]$

The high-fidelity UQ method has been used to estimate the full PDF of the QoI J for the baseline profile and for the RDO optimum. Such a comparison is presented in Figure 6, showing the success of the RDO carried out, since the PDF calculated for the optimal solution has lower mean and standard variation than the one for the baseline geometry. This result is summarized in Table 3, reporting the statistical moments of both the PDFs: it appears that the RDO can reduce $E[J]$ by 20% and $STD[J]$ by 27.2%. The optimal solution and the baseline profile are compared in Figure 7: it appears that the RDO has transformed the starting geometry in a front-loaded profile, transferring the blade load to the first part of the blade. Moreover, the RDO gives a converging-diverging shape to the profile.

Table 3: Statistical moments of the PDF of QoI J for the baseline profile and the RDO optimum

| Quantity | Baseline | RDO Optimum | $\Delta\%$ |
|----------|----------|-------------|------------|
| $E[J]$ | 8.307 | 6.646 | -20.0% |
| $STD[J]$ | 3.824 | 2.784 | -27.2% |

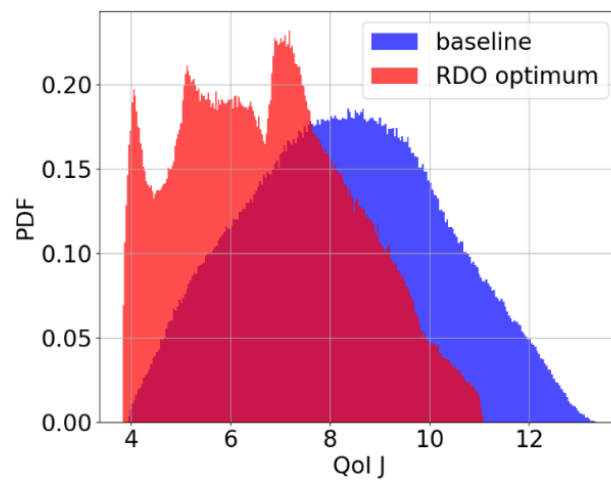


Figure 6 Comparison of the PDF of QoI J for the baseline profile and for the RDO optimal solution

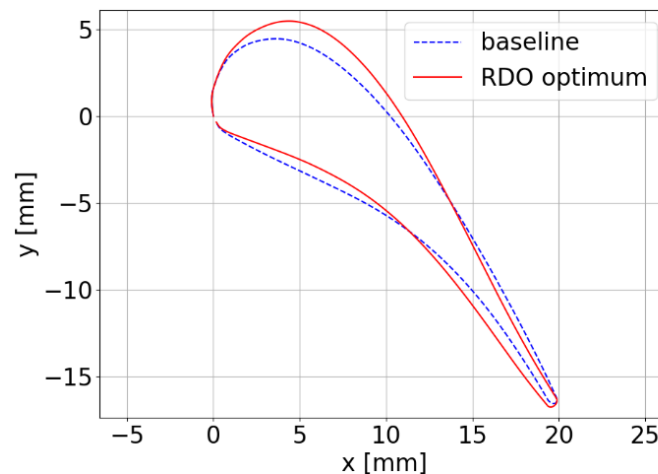


Figure 7: Comparison of the baseline with the optimal design

Finally, a CFD simulation is performed for both the profiles at the deterministic boundary conditions in Table 4. The results are depicted in Figure 8 and Figure 9.

Table 4: Deterministic boundary condition for the CFD analysis performed on both geometries

| | | |
|------------|------------|-----------|
| $P_{T,in}$ | $T_{T,in}$ | P_{out} |
| 28.9 bar | 277.3 degC | 10.05 bar |

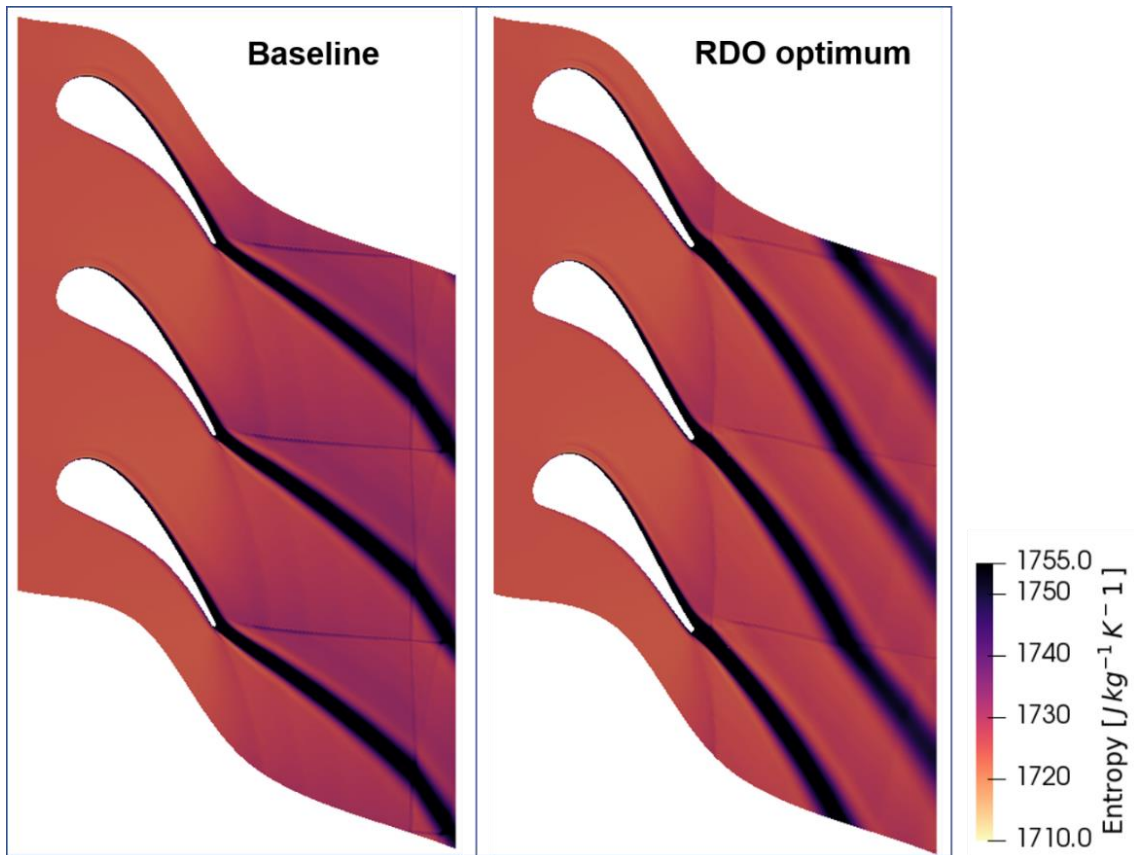


Figure 8: Comparison of the entropy field between the baseline and the RDO optimal geometry

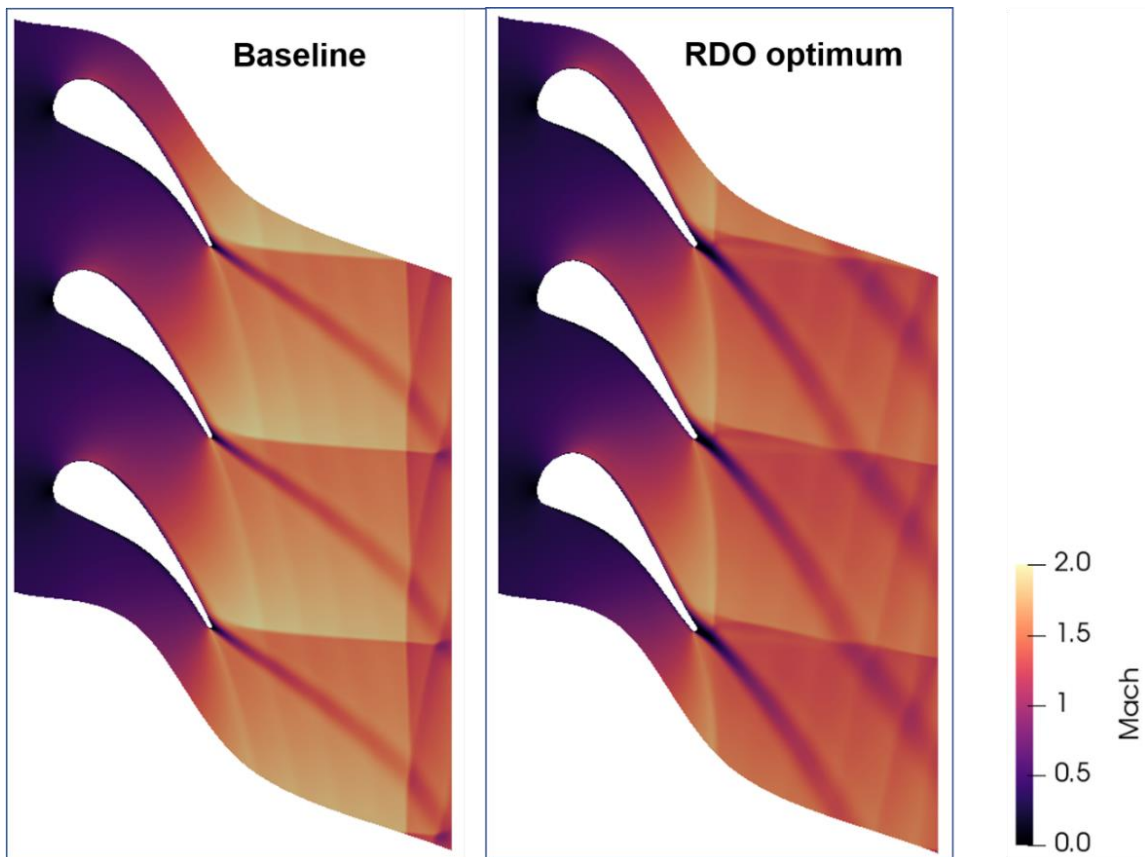


Figure 9: Comparison of the Mach number distribution between the baseline and the RDO optimum

From the analysis of Figure 8, one can identify in both profiles three main dissipation zones: the boundary layer over the blade profile, the trailing edge and the downstream region. The first one is an expected effect of the fluid viscosity and it has a lower influence on the account of losses than the other two phenomena. Figure 9 shows that the blade is subject to a large pressure ratio, which is achieved by means of a post-expansion. Immediately before the trailing edge, the Mach number is 2 on the suction side of the baseline profile, generating a “fish-tail shock system” that propagates downstream with large effects on the resulting flow field: the shock generated on the pressure side reaches the suction side of the adjacent blade, it is reflected and it increases its strength merging with the shock wave generated on the suction side. Finally, it interacts with the wake coming from the adjacent blades. The RDO optimal solution shows the same phenomenology just presented as well, but with a lower intensity, since the transfer of the blade load on the first part of the profile allows to reduce the maximum Mach number on the suction side of the blade to the value of 1.8.

Table 5 summarizes three performance parameters for both geometries, namely Δs , that is the entropy increase between the inlet at the outlet sections of the domain, the corresponding total pressure drop ΔP_T and the pressure loss factor $\gamma_P = \Delta P_T / (P_{T,in} - P_{out})$.

Table 5: Comparison of performance parameters for both geometries

| Geometry | Δs [$J\ kg^{-1}K^{-1}$] | ΔP_T [Pa] | γ_P [%] |
|-------------|-----------------------------------|-----------------------|----------------|
| Baseline | 10.468 | 290443 | 15.41% |
| RDO Optimum | 9.504 | 267093 | 14.17% |

The convergence of the RMS residuals for the mass, the momentum (in directions X and Y) and energy is plotted in Figure 10, while the check of the grid convergence is presented in Figure 11, showing the estimation of the quantity \overline{M}_{out} obtained on the coarse, the medium and the fine grids: rigorously speaking, it appears that this result on the fine grid is not completely converged and a more refined mesh would have been necessary to obtain a more grid-independent solution. Nevertheless, the reduced difference between the solution calculated on the fine grid and on the medium one, allows the use of this last one for the simulations solved during the RDO. On the other hand, the comparison between the baseline geometry and the optimal solution has been carried out on the fine mesh.

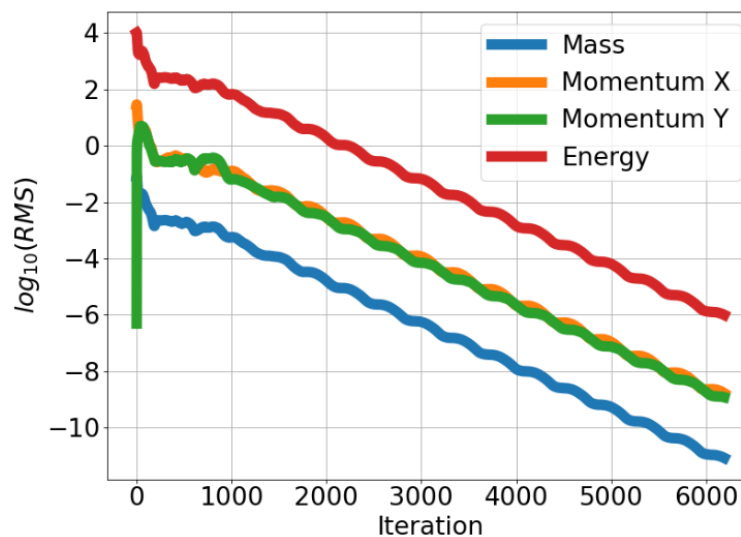


Figure 10: Convergence of residuals

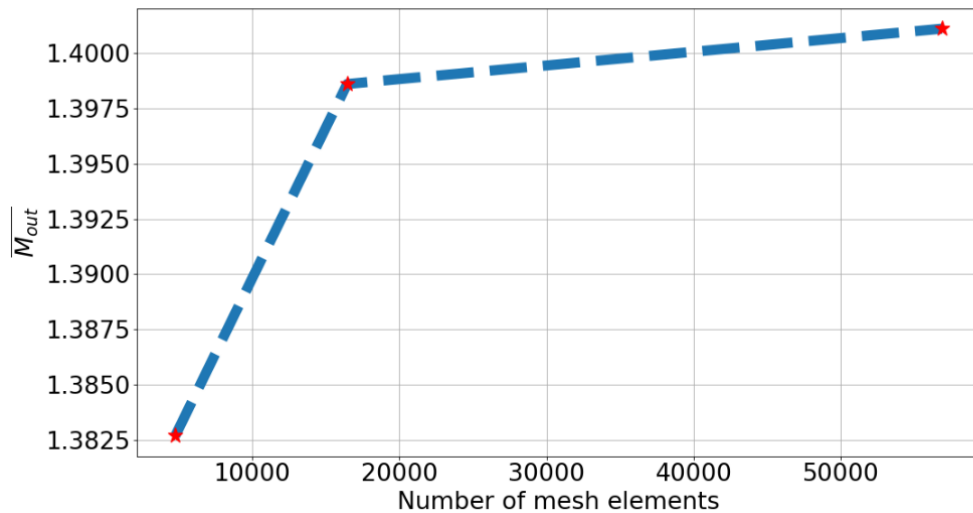


Figure 11: Convergence to solution of quantity \overline{M}_{out} vs. mesh refinement

5 CONCLUSIONS

A promising multi-fidelity RDO strategy has been successfully applied to the efficient 2D design of the first nozzle of an ORC turbine for high temperature waste-heat recovery, whose working conditions are affected by aleatory uncertainty both at the inlet and at the outlet. This uncertainty defines a large operating interval for the turbomachinery. The optimization converges after only 1271 CFD simulations to an optimum solution, ensuring improved and stable performance over the whole considered operating range: with respect to the baseline geometry, the expected value of the PDF of the entropy generation along the cascade is reduced by 20.0% and the standard deviation by 27.2%.

Future works will focus on the application of the presented RDO strategy to the optimization of a 3D turbine blade or of a multi-cascade system with a mixing plane interface.

NOMENCLATURE

| | | |
|------------|---|---------------------------------------|
| E[J] | Expected value of the PDF of the QoI | - |
| P | Pressure | (bar) |
| PDF | Probability distribution functions | - |
| QoI | Quantity of Interest | - |
| RDO | Robust design optimization | - |
| s | Entropy | (J kg ⁻¹ K ⁻¹) |
| STD[J] | Standard deviation of the PDF of the QoI | - |
| T | Temperature | (degC) |
| UQ | Uncertainty quantification | - |
| WHR | Waste heat recovery | - |
| ΔP | Difference of pressure | (Pa) |
| δ | Vertical displacement of FFD control points | (% in the lattice reference system) |
| γ_P | Pressure loss factor | (%) |

Subscript

| | |
|-----|--------|
| in | inlet |
| out | outlet |
| T | total |

REFERENCES

Bianchi, G., Panayiotou, G.P., Aresti, L. et al., 2019, Estimating the waste heat recovery in the European Union Industry. *Energ. Ecol. Environ.* 4, 211–221 (2019).

- Bufi, E.A. and Cinnella, P., 2016, Robust optimization of supersonic ORC nozzle guide vanes, *J. Phys.: Conf. Ser.*, vol.821, n. 012014.
- Deb, K., Pratap, A., Agarwal, S. et al., 2002, A Fast and Elitist Multiobjective Genetic Algorithm: NSGA-II, *IEEE transactions on evolutionary computation*, vol. 6, no. 2.
- Economon, T. D. et al., 2016, SU2: An Open-Source Suite for Multiphysics Simulation and Design, *AIAA Journal*, vol. 54, no. 3, pp. 828–846.
- Exergy, 2021, Waste Heat Recovery references, consulted on April 19th, 2021, available online: <https://www.exergy-orc.com/application/heat-recovery-from-industrial-process>
- EU Parliament, 2018, Directive (EU) 2018/2002 of the European Parliament and of the Council of 11 December 2018 amending Directive 2012/27/EU on energy efficiency.
- Geuzaine, C. and Remacle, J.-F., 2009, Gmsh: a 3-d finite element mesh generator with built-in pre and post-processing facilities, *Int. J. for Numerical Methods in Engineering*, vol. 79, no. 11, p. 1309–1331.
- Hazelton, M.L., Methods of moments estimation, in *Int. Enc. of Stat. Sc.*, Ed. Springer, pp. 816–817.
- IEA, The International Energy Agency, 2018, World Energy Outlook 2018, Paris.
- IEA, The International Energy Agency, 2020, Energy Efficiency 2020, IEA, Paris.
- Jameson, A., 2017, Origins and further development of the Jameson–Schmidt–Turkel scheme, *AIAA Journal*, vol. 55, no. 5, pp. 1487–1510.
- Keane, A.J., 2006, Statistical improvement criteria for use in multiobjective design optimization, *AIAA Journal*, vol. 44, no. 4, pp. 879–891.
- Levi, P., Vass, T., Mandovà, H. et al., 2020, Tracking Industry 2020, IEA, Paris, available online: <https://www.iea.org/reports/tracking-industry-2020>
- Liu, Q., Lei, Q., Xu, H. et al., 2018, China’s energy revolution strategy into 2030, *Resources, Conservation and Recycling*, vol. 128, pp. 78-89, <https://doi.org/10.1016/j.resconrec.2017.09.028>.
- Mahmoudi, A., Fazli, M. and Morad, M.R., 2018, A recent review of waste heat recovery by Organic Rankine Cycle, *Applied Thermal Engineering*, Vol. 143, pp. 660-675.
- Menter, F. R., 1994, Two-equation eddy-viscosity turbulence models for engineering applications, *AIAA Journal*, vol. 32, no. 8, pp. 1598–1605.
- Ormat, 2021, Waste Heat Recovery references, consulted on April 19th, 2021, available online: <https://www.ormat.com/en/projects/all/main/?Country=0&Seg=0&Tech=8>
- Papapetrou, M., Kosmadakis, G., Cipollina, A. et al., 2018, Industrial waste heat: Estimation of the technically available resource in the EU per industrial sector, temperature level and country, *Applied Thermal Engineering*, vol. 138, pp. 207-216.
- Peng, D.Y. and Robinson, D. B., 1976, A new two-constant equation of state, *Industrial & Engineering Chemistry Fundamentals*, vol. 15, no. 1, pp. 59–64.
- Razaaly, N., Persico, G., Gori, G. and Congedo, P.M., 2020, Quantile-based robust optimization of a supersonic nozzle for ORC turbines, *Applied Mathematical Modelling*, vol. 82, pp. 802 – 824.
- Serafino, A., Obert, O. and Cinnella, P., 2020a, Multi-Fidelity Gradient-Based Strategy for Robust Optimization in Computational Fluid Dynamics, *Algorithms*, vol. 13(10), n. 248.
- Serafino, A., Obert, B., Vergé, L. and Cinnella, P., 2020b, Robust optimization of an organic Rankine cycle for geothermal application, *Renewable Energy*, vol. 161, p. 1120-1129.
- Sederberg, T. W. and Parry, S. R., 1986, Free-form deformation of solid geometric models, *SIGGRAPH Comput. Graph.*, vol. 20, no. 4, pp. 151–160.
- US CONGRESS, 2021, Consolidated Appropriations Act, 2021. Available online: <https://www.congress.gov/116/bills/hr133/BILLS-116hr133enr.pdf>
- Taguchi, G., 1987, System of experimental design: engineering methods to optimize quality and minimize costs. UNIPUB/Kraus International Publications.
- Turboden, 2021, Waste Heat Recovery references, consulted on April 19th, 2021, available online: <https://www.turboden.com/solutions/1053/waste-heat-recovery>
- Wikle, C.K. and Berliner, L.M., 2007, A Bayesian tutorial for data assimilation, *Physica D: Nonlinear Phenomena*, vol. 230, no. 1, pp. 1–16.